

**Estimation of the Atmospheric Boundary Layer height during
different atmospheric conditions: A comparison on reliability of
several methods applied to lidar measurements**

Toledo, D.^{1,2}, Córdoba-Jabonero, C.¹, Adame, J. A.¹, De la Morena, B.¹,
Gil-Ojeda, M.¹

¹*Instituto Nacional de Técnica Aeroespacial (INTA), Atmospheric Research and
Instrumentation Branch, Torrejón de Ardoz, 28850-Madrid, Spain,*

²*Department of Physics, University of Oxford, Parks Rd, Oxford OX1 3PU, UK.*

Corresponding Author: Carmen Córdoba-Jabonero, Instituto Nacional de Técnica
Aeroespacial (INTA), Ctra. Ajalvir km.4, Torrejón de Ardoz-28850, Madrid, Spain.
Phone/fax: +34 915201294/+34 915201633. E-mail: cordobajc@inta.es

Estimation of the Atmospheric Boundary Layer height during different atmospheric conditions: A comparison on reliability of several methods applied to lidar measurements

The performance of six numerical methods usually used to determine the Atmospheric Boundary Layer (ABL) height from lidar measurements was investigated under different atmospheric conditions: results were compared with those obtained from radiosoundings to analyse their reliability for ABL-height retrievals. The selected methods were the gradient method (GM), the logarithm gradient method (LGM), the inflection point method (IPM), the wavelet covariance transform (WCT), the centroid/variance method (VM) and the cluster analysis (CA). Lidar measurements were carried out in the frame of the “Atmospheric Minor Species relevant to the Ozone Chemistry” (AMISOC) project during a multi-instrument campaign conducted at the INTA/Atmospheric Observatory “El Arenosillo” (INTA/ARN) in south-western Spain from 15 May to 20 June 2012. The goal of this work is to analyse the performance and robustness of the different lidar methods in this region, characterized by particular atmospheric conditions. In particular, both events of sea-land breeze regimes and episodes of Saharan dust intrusions were studied. In most days, similar results were obtained by all lidar methods in the events of sea-land breeze regimes, presenting relative absolute differences between lidar and radiosounding retrievals below 12 % in average. However, big discrepancies between lidar and radiosounding retrievals are found when residual layers are present in the measurements. In such cases, the vertical extension of lidar and radiosounding profiles must to be limited to the altitude of the residual layer bottom.

In a second analysis, focused on diurnal variability in the ABL heights under non-dusty (ND) and dust (DD) conditions, the methods were tested against intensive radiosoundings launched every 4 hours over 2

days. Under ND conditions, the best results were achieved for the LGM, presenting a mean of the relative absolute differences respect to radiosounding measurements of 10 %. The rest of methods also provided good results with relative differences below 20 % in average. Under DD conditions, however, an increase of the relative differences is found with mean values of up 32 %. In this case, best results are given by CA with a mean relative difference of 20 %. Despite the limited data set used in this work, results show that unlike the ND conditions for which all lidar methods provide good results respect to radiosounding retrievals, under DD conditions the election of the lidar method is a key factor for ABL estimation. However, we remark the need of extending our analysis to longer periods of time to better characterize the differences observed in this work.

Keywords: ABL; numerical methods; sea-land breeze regimes; lidar; radiosoundings; Saharan dust.

1 Introduction

The Atmospheric Boundary Layer (ABL) is defined as the lowest part of the troposphere that is directly influenced by the Earth's surface on a timescale of one hour or less (Stull, 1988). The ABL is affected by orography, land cover, weather conditions, and solar radiation in particular; thus, the layer evolves throughout the day. After sunny and clear sky conditions over land, the formation of stable layers (thermal inversions) is typical as the ground cools overnight. In the daytime, surface heating drives convective processes that generate unstable conditions (forming a mixing layer). Air pollutants are released into the ABL, where they mix with upper-level air via dispersion processes, according to the ABL structure and turbulence. Therefore, robust knowledge of ABL dynamics is crucial for weather forecast modeling and air pollution studies (Seibert et

al., 1998, 2000).

Many different instruments and techniques have been used to estimate ABL heights. Radio soundings are the most reliable instruments because they use both potential temperature and humidity (Heffter 1980; Stull 1988). Unfortunately, the daily schedule of radiosonde launchings is, at most, twice per day. Hence, alternative instrumentation must be used on a daily basis. Active remote sensing systems, such as lidars, have been used to estimate ABL heights. Lidars offer two main advantages: a) the ability to detect the large aerosol gradients in the atmosphere that delimit the ABL and the Free Troposphere (FT), i.e., identification of the ABL top height; and b) the ability to operate on a continuous mode with a high temporal resolution.

Two types of methods have been used to determine the top of the ABL: 1) methods that find a sharp spike in the lidar signal in the transition zone (TZ) between the ABL and the FT; and 2) methods based on statistical analysis. The methods that use the first approach assume that the aerosol concentration at heights below the ABL top is significantly higher than that in the FT. For instance, Melfi et al. (1985) and Boers et al. (1988) defined the ABL top as the height where the backscattered lidar signal drops below a given threshold. Hence, these methods have the disadvantage of requiring an appropriate selection of this threshold value, which depends on the lidar system and on the weather conditions. For that reason, they are discarded in this work.

The most common procedure used to detect the ABL height in the backscattered lidar signal profile is an analysis of its derivative. There are three ways to analyze the derivative of the lidar signal with respect to height: the simple derivative (Hayden et al.,

1997; Flamant et al., 1997), the derivative of the logarithm of the signal (Senff et al., 1996), and the second derivative (Menut et al., 1999). These methods are good candidates for estimating the ABL top height because the total time processing to retrieve the heights is very low. However, the methods are affected by noise, and small-scale structures in lidar signals introduce large gradients unrelated to the ABL top height. Indeed, results obtained by derivative methods strongly depend on the value of the lidar signal gradient at a given point.

The wavelet covariance transform (WCT) approach is less affected by the signal noise and is also used for ABL top determination (Steyn et al., 1999; Cohn and Angevine, 2000; Davis et al., 2000; Hägeli et al., 2000; Brooks, 2003). WCT, also called Haar wavelet transform, provides a multi-scale local gradient analysis of the lidar signal to isolate the spikes due to aerosol concentrations. A recently published comparative study (Pal et al., 2010) shows that the ABL height obtained by the Haar wavelet method ranges between the values estimated by the derivative of the logarithm of the signal and the second derivative. Notably, these methods assume that the transition range in the backscattered lidar signal from the ABL to the FT closely corresponds to the temperature inversion zone (Brooks, 2003).

However, methods based on statistical analysis are related to large temporal variability in the aerosol concentration in the TZ because clear air masses from the FT are mixed with those from the ABL. A more widely applied method for ABL estimation is the centroid/variance method (VM) (Hooper and Eloranta, 1986; Piironen and Eloranta, 1995; Menut et al., 1999). This approach estimates the ABL height by using the variance of the lidar signal over a particular time period. As a result, a high

variability in the backscattered lidar signal in the TZ reveals a local maximum in the variance profile at that height.

Additionally, cluster analysis (CA) is a method used for lidar-derived ABL height estimations (see details in Toledo et al., 2014); the method combines both of the previous approaches. CA is based on assembling a set of objects into groups (Anderberg, 1973), where the objects in the same cluster are similar and objects in different clusters are dissimilar (Balling, 1984). Hence, the ABL top height is identified by analyzing the vertical distribution of the different clusters (Toledo et al., 2014).

In this work we compare ABL estimated from lidar measurements using the methods mentioned above with those obtained from radiosounding measurements under the particular atmospheric conditions found in the INTA/Atmospheric Observatory “El Arenosillo”; (1) events of sea-land breeze regimes; (2) dust intrusion events. The goal of this comparison is to study the performance of the different lidar methods under these atmospheric conditions that directly influence on ABL.

2 Methodology

2.1 AMISOC-ARN campaign: area description and lidar measurements

In the framework of the “Atmospheric Minor Species relevant to the Ozone Chemistry at both sides of the jet” (AMISOC) project, lidar measurements were performed during a multi-instrument campaign conducted at the “El Arenosillo” Atmospheric Observatory (ARN, 37.1°N 6.7°W, 40 m a.s.l.), which is managed by the

Instituto Nacional de Técnica Aeroespacial (INTA). In particular, one of the objectives of that project is to evaluate the impact of the ABL on surface ozone levels under dusty conditions (Adame et al., 2015). Hence, ABL height estimation is specifically addressed within the AMISOC project.

INTA temporarily deployed a Micro Pulse Lidar v.3 (MPL-3) system at the ARN station from 20 May to 15 June 2012 to measure ABL heights. The ARN observatory is located in a rural environment, the Doñana National Park, in the southwestern Iberian Peninsula; it is approximately 1 km from the Atlantic Ocean. Air masses originate from various regions, such as the Atlantic Ocean, Europe and African deserts, and often cross this area. Thus, the ABL can be studied for a wide range of atmospheric conditions. In this work, dust intrusions in the area during AMISOC-ARN are specifically examined.

The lidar system used during the AMISOC-ARN campaign is the Micro Pulse Lidar v.3 (MPL-3) usually in routine operation within the NASA Micro Pulse Lidar NETwork (MPLNET, <http://mplnet.gsfc.nasa.gov>) at the Santa Cruz de Tenerife site (Canary Islands, Spain), managed in collaboration with AEMET (Spanish Meteorological Agency). The system is a single-wavelength (523 nm), high-repetition (2500 Hz), low-power ($\sim 7 \mu\text{J}$), eye-safe backscatter lidar that is commercially available, and capable of determining the range of aerosols and clouds in a fully unattended operation mode. The raw signals were corrected for several factors (Campbell et al., 2002) that affect the instrument. A more detailed description of this system and corrections can be found in Cordoba-Jabonero et al. (2011). In particular, the full overlap of the system is reached at around 3 km height, with uncertainty values of 10–

30% from 300 m height up, increased up to 60% at lower altitudes. Hence, data below 300 m height a.g.l. are usually disregarded in lidar inversion procedures to obtain optical properties of aerosols. However, the ABL retrievals (see next Sect 2.2) are applied to the lidar range-corrected signals (RCS) (no other lidar inversions are needed for ABL top height determination) from ground level up. MPL-3 measurements were performed on a daily basis, with a 1-min integration time and a vertical resolution of 15 m. These 1-min lidar RCS profiles were averaged over 10 minutes for both the variance calculations and signal-to-noise (s/n) ratio enhancement; thus, 6 RCS profiles were obtained for each hour (144 RCS profiles per day).

2.2 Methods applied to lidar measurements for ABL height determination

Since the methods used in this work are well known, only a brief description is presented. The methods used for ABL height estimation are the gradient method (GM), the logarithm gradient method (LGM), the inflection point method (IPM), the wavelet covariance transform (WCT), the centroid/variance method (VM) and the cluster analysis (CA). The ABL height is defined by GM and LGM as the altitude where is found the negative minimum of the first derivative of the RCS and the negative minimum of the first derivative of the RCS logarithm, respectively. For the IPM, the altitude is given where the curvature of the lidar RCS experiences a sign change. In particular, when applying the IPM, Menut et al. (1999) used the absolute minimum of the second derivative of the RCS, whereas Sicard et al. (2006) defined the ABL top as the altitude of the minimum found below the ABL height retrieved by GM.

The WCT method basically analyses the gradients present in the RCS by using a wavelet function, particularly the Haar function (see, e.g., Brooks, 2003), depending on

the translation and dilation parameters. Translation defines the height of the Haar function, and dilation represents the vertical extent of the function. Hence, the ABL top height is located where the maximum WCT value is found by applying appropriate values of those two parameters, depending on the depth of the TZ. Signal noise dominates the vertical WCT profiles for low dilation values; alternatively, the WCT maximum represents the ABL height for dilation values close to the depth of the TZ between the ABL and the FT.

The last two methods, VM and CA, are based on statistical analysis to define the ABL height. Based on the high temporal variability of the aerosol concentration in the TZ, the ABL height is identified by VM as the lowest height position of a local maximum in the temporal variance profile of RCS. The CA method is based on the assembling a set of objects into groups (Anderberg, 1973), where the objects in the same cluster are similar and objects in different clusters are dissimilar (Balling, 1984). In particular, the distance between objects is the measure of the similarity between clusters. These distances are based on single or multiple dimensions, where each dimension represents a condition that groups the objects. Each dimension is represented by the height, the lidar RCS and the variance for a given period. Clusters can be formed using these distances with normalized values of all the variables. Therefore, the distribution of the aerosols in the atmosphere and variations in their concentrations can be studied simultaneously using this method. The ABL top height is defined as the height where a change from one cluster to another is observed (Toledo et al., 2014).

2.3 Meteorological observations: surface and profiles

Local weather conditions were determined during the AMISOC-ARN campaign.

Temperature, relative humidity, pressure, rainfall, wind speed and wind direction data were registered by Vaisala 520WXT sensors located at three heights (10, 50 and 100 m a.g.l.) on a 100-m high tower. In addition, meteorological profiles were obtained by using Vaisala radiosonde launches. Vertical measurements of temperature, pressure, humidity and wind (direction and speed) were registered with an accuracy/resolution of $<0.2^{\circ}\text{C}/0.1^{\circ}\text{C}$, $<0.6\text{ hPa}/0.1\text{ hPa}$, and $<5\%/1\%$, respectively. The uncertainty in the wind speed and direction is 0.15 m s^{-1} and 2 degrees, respectively. All the soundings experienced a mean flight time of approximately 80 minutes and reached an altitude of approximately 22-23 km.

A total of 26 radiosoundings were launched on a daily basis at approximately 11:00 UTC. Additionally, two intensive launching schedules were planned for analyzing the robustness of the different methods throughout the day in relation to Saharan dust conditions. Non-dusty (ND) and dusty (DD) conditions were observed on 23-24 May and 31 May-1 June 2012, respectively. The criterion to identify the DD conditions, as adopted from Córdoba-Jabonero et al. (2011), is based on AERONET (AErosol Robotic NETwork, www.aeronet.nasa.gov) parameters: DD conditions are fulfilled for threshold Aerosol Optical Depth (AOD) values higher than 0.2 and Angstrom Exponents (AEx) lower than 0.5 (predominance of coarse particles). Otherwise, the present conditions correspond to a ND case. The AOD for the DD period ranges from 0.24 to 0.43, and with AEx values below 0.5, while for the ND period we found AODs less than 0.15 and AEx values greater than 0.9 (Adame et al., 2015). In both intensive 2-day periods, the first radiosounding was launched at approximately 11:00 UTC, followed by 5 radiosoundings every 4 hours. In general, the sunshine

duration is approximately from 05:30 UTC (sunrise) to 19:30 UTC (sunset); hence, convective mixing in the ABL becomes relevant during this period.

Depending on convective conditions, two different approaches were used to estimate the ABL height from the radiosounding measurements. Under convective conditions, the ABL top is obtained by averaging the heights estimated from both the potential temperature and specific humidity profiles. The ABL top is defined as the height where the maximal/minimal vertical gradient of the potential temperature/specific humidity is found (Oke, 1988; Sorbjan, 1989; Garratt, 1992). Above this altitude, the atmosphere can be considered the Free Troposphere (FT). Under surface inversion conditions, the ABL height is identified as the maximum height of the surface inversion layer.

To determine the robustness of each method, the ABL heights are calculated by all the proposed methods (GM, VM, WCT, LGM, IPM and CA) and are compared with those obtained from the daily radiosoundings. Hence, the absolute differences between the values obtained by each method and by the radiosounding retrievals are presented in terms of their mean and one-standard-deviation (1σ) values. Those differences were taken in absolute value in order to avoid negative values in the calculation of the mean. In addition, we did not observe in our study any lidar method providing systematically ABL altitudes above or below radiosounding retrievals. The confidence of each method in retrieving the ABL height under different atmospheric conditions is also analyzed in specific situations: 1) particular sea-land breeze conditions in which the ABL evolution is determined during the AMISOC-ARN campaign with respect to discrete daily radiosoundings (launched at around 11 UTC); and 2) dissimilar aerosol scenarios under

DD and ND conditions in which the ABL evolution during the day (day/night variations) is determined with respect to intensive radiosoundings (launched every 4 hours for two consecutive days).

3 Results and discussion

3.1 ABL evolution during the AMISOC-ARN campaign: identification of sea-land breeze conditions

Surface meteorological observations indicate that the lower atmosphere was governed by synoptic flows for only three days (~10% of the total campaign period) and by mesoscale processes for the remaining period. Two well-known sea-land breeze patterns usually occur in this area, classified as pure and non-pure. Pure breezes occur with flows (diurnal and nocturnal) perpendicular to the coast line, whereas non-pure breezes occur under synoptic forcing conditions (nocturnal) that not quite perpendicular to the coast (Adame et al., 2010). According to this criterion, 12 days were identified as pure breezes and 14 days as non-pure breezes. Figure 1 shows the surface weather conditions (temperature, relative humidity and wind) for pure (22 to 25 May 2012) and non-pure (6 to 8 June 2012) conditions.

FIGURE 1

Pure breezes reflect flows perpendicular to the coastline and well-established daily cycles of temperature and humidity. An increase in the temperature is observed each day due to the recirculation of the same air. Non-pure breezes exhibit nocturnal

flows that are not perpendicular to the coastline and that are associated with synoptic forcing conditions (higher wind speeds than pure breeze regimes); in this case, the daily cycles of temperature and relative humidity are not clear.

The ABL heights obtained using each method and from the radiosoundings as well as the absolute differences (absDiff) between the ABL height values calculated using the six methods and those obtained from radiosoundings are shown in Figure 2; the error bars represent the standard deviations of the mean ABL top heights calculated by each method from the ten 1-min lidar profiles used in the averaging procedure. The bands limited by dashed lines represent the corresponding breeze regime identified for each day to distinguish pure (indicated by double arrows) and non-pure cases (no arrows). Since the comparison between both instruments could be affected by the velocity and direction of the wind a correlation analysis between these parameters and the absolute and relative differences between the radiosounding and lidar retrievals was performed. In this analysis we did not find an increase of such differences for the days with a higher wind speed (maxima wind speed around 9 ms^{-1}) or for the days with a wind direction near 220° N (angle between the North and the line perpendicular to the coastline). Therefore, balloon drifts do not noticeably affect the comparison illustrated in Figure 2. The temporal resolution of radiosounding measurements was of 5 seconds, resulting in a vertical resolution between 12 and 34 m at altitudes near ABL height.

FIGURE 2

Higher ABL tops are observed under pure breeze conditions (see Fig. 2a). Mean values of $1508 \pm 374 \text{ m}$ and $1265 \pm 290 \text{ m}$ are obtained from the radiosoundings under

pure and non-pure breezes, respectively. Non-pure breeze conditions are developed with lower surface temperatures and higher wind speeds than pure breezes with synoptic forcing at the upper levels (Hernandez-Ceballos, et al., 2013). These conditions are less favorable for the development of convective processes; lower mixing heights are observed in non-pure cases than in pure cases. In most days, the ABL height was retrieved under cloud or residual layer free conditions for which all lidar methods and radiosounding measurements provided similar altitudes. An example of one of those days is illustrated in Figure 3 that shows the time variation of lidar RCS on 21 May 2012, the ABL height estimated by GM and VM, and the radiosounding ABL height estimated for that day. We can observe that both lidar methods are in agreement with differences below 100 m in most ABL retrievals (similar results were found for the rest of lidar methods). However, Figure 2 shows big deviations between VM and the rest of retrievals for the days 24-25 May, 29 May and 12 June. These differences are caused by the presence of residual layers during the time period when the radiosounding was launched. An example is illustrated in Figure 4, where the white arrow indicates a residual layer between 9 UTC and 11:40 UTC. In this case, we can observe that GM and VM provide similar ABL altitudes except between 11 UTC and 11:40 UTC (similar differences are also found between VM and the rest of lidar methods). The main reason of such differences is the fact that all lidar methods except VM provide the altitude of the residual layer. As observed in Figure 4, at around 11:00 UTC the bottom of the residual layer lies just above the ABL height. At that moment, all lidar methods except VM provide the top height of the residual layer. Radiosounding measurements also provide the altitude of the residual layer as result of its humidity gradient. However, VM estimates correctly the altitude of the growing ABL, being therefore the most reliable method in this analysis when residual layers are present.

FIGURE 3

FIGURE 4

Excluding these days, similar estimates are derived by all lidar methods. Among the pure-breeze cases, the smallest difference is found for the IPM with a value below 15 m and the largest difference is found for the VM with a value of about 350 m. However, the smallest absDiff maximum is found for WCT with a value of 197 m. This feature is very important to analyze for evaluating the stability of each method because the deviation between each method and radiosounding retrievals is highly dominated by the maximum absDiff value. Under non-pure breeze conditions, almost all of the methods present small differences in ABL top heights with respect to the heights retrieved by the radiosoundings. In particular, the smallest and largest absDiff values are obtained for WCT, respectively (see Fig. 2b, bottom panel). The smallest maximum absDiff value is obtained for CA (111 m). The ABL top heights derived by the VM under non-pure breeze conditions are consistent with the radiosounding retrievals. In particular, the smallest absDiff value (148 m) is found on 3 June by the VM, whereas a value greater than 270 m is obtained for the other methods.

The mean absolute relative difference (mean reDiff), mean absDiff and the one standard deviation (1σ) obtained by each method for all the pure and non-pure breeze cases, as well as for the overall period, are shown in Figure 5 (excluding the days 24-25 May, 29 May and 12 June). These results represent the robustness of the different methods in determining the ABL top height.

FIGURE 5

Under pure-breeze conditions, WCT and LGM present the lowest values of both the mean absDiff and reDiff, whereas the VM reports the highest mean absDiff (> 136 m) with a mean reDiff of 0.09. Low mean absDiff and reDiff values are also found for CA, 116 m and 0.089, respectively. Among the derivative methods, best results are given by LGM with mean absDiff and reDiff values of 103 m and 0.08. This result can clearly be explained by the enhancement of the aerosol contrast obtained by taking the logarithm of the RCS lidar signal. By examining the 1σ values, the WCT shows the smallest value. However, the other methods are reasonably consistent according to their mean absDiff values. In general, all methods are in agreement with the radiosounding retrievals for this period with mean absDiff and reDiff values below 137 m and 0.095, respectively; the best results are obtained for WCT and LGM.

The results obtained for non-pure breeze cases using the GM, LGM, IPM, VM, WCT and CA are very similar to those found under pure breeze conditions with mean absDiff and reDiff values below 130 m and 0.11, respectively. Specifically, a mean absDiff value lower than 100 m is obtained for the VM, whereas a value of 130 m is found for the IPM. In this period best results are given by VM although the differences in the mean absDiff respect to the other methods are below 30 m. By analyzing the overall period (third panel of Figure 5), the ABL altitude retrieved by lidar methods are in good agreement with radiosounding estimations. The best results are obtained by LGM with a mean absDiff value of 107 m. However, we remark that the rest of methods provide mean absDiff values below 128 m. In summary we found that all lidar methods provided similar results with differences below 40 m in average. However,

limitations are found when residual layers are present in the measurements. Under such conditions, VM provides the most reliable ABL retrievals.

3.2 ABL evolution during the day: influence of the aerosol conditions

Two aerosol conditions were identified and selected during the AMISOC-ARN campaign by intensive radiosonde launchings: 24-25 May 2012 and 31 May-01 June 2012 under non-dusty (ND) and dusty (DD) conditions, respectively. Both periods featured pure-breeze flow regimes most of the time. For the first intensive period, a total of 7 radiosoundings were launched every 4 hours. Because of the low ABL height value obtained for the radiosounding launched at 04:00 UTC, this case is not included. In the second intensive period, a total of 6 radiosoundings were launched every 4 hours (unfortunately, the last radio sounding launched at approximately noon failed).

As mentioned in section 3.1, residual layers were present for the days 24-25 May, resulting in vertical or temporal lidar signal gradients at altitudes above the ABL height. In this regard, we found necessary to limit the top of lidar and radiosounding profiles to altitudes below the bottom of the residual layers. The ABL heights obtained by the six methods and those retrieved from the radiosounding data during the ND and DD periods are shown in Figures 6a and 7a, respectively.

FIGURE 6

FIGURE 7

During the ND period, the first two and the last radiosoundings were launched

only under convective conditions; however, only the first radiosounding in the DD period experienced these conditions. For these cases, the ABL height values were higher than those for the rest of the intensive period, as expected for atmospheric convection. The error obtained during both periods for the different methods decreased as the convective conditions diminished, likely associated with more nocturnal stability. Indeed, under these conditions, the ABL presents a strong static stability; hence, its vertical variability over time is very low. Although all of the methods well reproduce the behavior of the ABL evolution during the day, differences are found with respect to the radiosounding retrievals.

In order to examine these discrepancies, the absolute differences (absDiff) between the ABL heights calculated using each method and those obtained from the radiosoundings under the ND and DD conditions are shown in Figures 6b and 7b. The smallest absDiff values are obtained for the ND period by the GM, LGM, VM and CA with values lower than 15 m, whereas the largest absDiff values correspond to the WCT (around 200 m). The smallest maximum absDiff value is found for IPM (117 m). In comparison with the results obtained during the discrete daily radiosounding period (see Sect. 3.1), similar results are found for the different lidar methods with absDiff values below 150 m in most cases. Regarding the derivative methods, a good agreement is found with respect to the radiosounding retrievals. During the DD intensive period (31 May-01 June 2012), the lowest and highest absDiff values are found by CA (11 m) and the VM (182 m), respectively, and the smallest maximum is obtained by CA and WCT (126 m).

In order to study the robustness of each method, the mean of reDiff and absDiff, and the corresponding 1σ values for the ND and DD periods are shown in Figure 8. For ND period, all methods provide reasonable mean values of reDiff and absDiff. In particular, best results are given by LGM with a mean reDiff of 0.10 and a mean absDiff of 58 m. By contrast, the highest values of these parameters for this period is given by WCT. For DD period, a remarkable increase of the mean values of reDiff and absDiff is observed for the derivative methods and VM. The lowest values of the mean absDiff and mean reDiff are found for the CA method, 56 m and 0.20, respectively.

In summary, results illustrated in Figures 6 and 8 show that for the ND period all lidar methods are in agreement with radiosounding retrievals with mean reDiff values below 0.21. However, for DD period CA is the only method providing a mean reDiff below 0.21 (see Figures 7 and 8). As mentioned in section 2.1, the overlap uncertainties increase at altitudes below 300 m. Therefore a similar analysis as that shown in Figure 8 was performed but considering only the cases with a ABL height above 300 m. The results are illustrated in Figure 9 where again CA provides the best result for DD period. A remarkable result is the noticeable decrease of mean reDiff values of the different lidar methods for the ND period. As reported by other authors (e.g. Pal, 2014), this decrease clearly shows that ABL height lidar retrievals are affected when overlap uncertainties become relevant. For the DD period the decrease in mean reDiff is smaller as result of the fewer number of cases of ABL heights below 300 m. Although results in Figure 8 indicate that lidar and radiosounding retrievals are in agreement, this analysis points out the need of decrease overlap errors at altitudes below 300 m to better characterize the ABL during nighttime.

FIGURE 8

FIGURE 9

4 Conclusions

ABL heights were determined during the AMISOC-ARN campaign by applying six mathematical methods to lidar measurements: the gradient method (GM), the logarithm gradient method (LGM), the inflection point method (IPM), the wavelet covariance transform (WCT), the centroid/variance method (VM) and the cluster analysis (CA). In order to analyze the performance of these methods, the ABL height results were compared with those derived from potential temperature and specific humidity profiles from radiosoundings.

This analysis of the robustness and capability of each method was based on that comparison under different atmospheric conditions: 1) sea-land breeze conditions, in which the ABL evolution during the entire AMISOC-ARN campaign was determined; and 2) dissimilar aerosol conditions, i.e., under dusty (DD) and non-dusty (ND) conditions.

First, each method was tested against discrete daily radiosounding measurements during the campaign for two types of coastal breeze regimes, and the convective conditions present in each case were examined. Excluding the cases with presence of residual layers, all methods provide similar results with relative absolute differences respect to radiosounding retrievals below 12 % in average. Despite that best results were given by LGM, VM and WCT, the differences respect to the others methods were smaller than

40 m in average. Since the vertical resolution of lidar and radiosounding measurements is of 15 and 34 m (maximum value found in this study), respectively, these results point out the need of improving the accuracy of ABL height estimation from these instruments to better analyze the differences observed in this period. Limitations of lidar methods were found in days with residual layers present at the radiosounding launch times. Under such conditions, we had to limit the vertical extension of lidar and radiosounding profiles to the altitude of the residual layer bottom.

Second, all of the methods were tested against intensive radiosounding retrievals under DD and ND conditions. Under ND conditions, best results are archived by GM, LGM, IPM and CA, with mean values of relative absolute differences of 16 %. However, the maxima difference in average between the different methods is of 35 m. Since the vertical resolution of radiosounding measurements ranges between 12 and 34 m, this result clearly shows the need of improve the vertical resolution of ABL height measurements to investigate those differences. CA provides the best results under dusty conditions with a relative difference of 20 % in average. The rest of methods provide mean values greater than 24 %.

In summary, under non-dusty conditions we found that all lidar methods are in agreement with radiosounding measurements. Though differences in lidar ABL height retrievals are found between the different methods, the vertical accuracy of the measurements clearly limits the interpretation of those differences. In spite of these limitations, results illustrated in Figures 5 indicate an increase in the differences under non-pure breeze conditions respect to the pure ones. A similar result is also observed in Figure 8, where a noticeable increase of the differences is given under the dusty

conditions. By comparing ABL altitudes under dusty and non-dusty conditions, we have observed lower ABL heights when dust intrusion events are present, observing even stable conditions in the early evening. Similarly, lower ABL altitudes are given under non-pure breeze conditions respect to pure conditions as result of the lower temperatures at surface. These increases in the differences indicate that the error in ABL estimation (using lidar measurements) increases as the mixing altitude decreases. However, we remark the need of extending this analysis carried out under these different atmospheric conditions for longer periods of time.

Acknowledgements

This work was supported by the Spanish Ministerio de Economía y Competitividad (MINECO) under grants CGL2011-24891 (AMISOC) and CGL2014-55230-R (AVATAR). The authors especially thank the INTA/Atmospheric Observatory “El Arenosillo” (ARN) staff for their valuable assistance and support in maintaining the lidar system and launching the radiosoundings.

References

- Adame, J. A., J. P. Bolívar, and B. de la Morena, 2010, Surface ozone measurements in the southwest of the Iberian Peninsula (Huelva, Spain). *Environ. Sci. Pollut. Res.*, **17**, 355–368.
- Adame, J.A., C. Córdoba-Jabonero, M. Sorribas, D. Toledo, M. Gil-Ojeda, 2015, Atmospheric boundary layer and ozone-aerosol interactions under Saharan intrusions observed during AMISOC summer campaign. *Atmos. Environ.*, **104**, pp. 205–216.
- Anderberg, M. R., 1973, *Cluster Analysis for Applications*. Academic Press, 359 pp.

548 Balling, R. C., Jr., 1984, *Classification in climatology*. Spatial Statistics and Models, G.
 549 L. Gaile and C. J. Willmott (Eds.), Reidel, 81-108.
 550 Boers, R., J. D. Spinhirne, and W. D. Hart, 1988, Lidar Observations of the fine-scale
 551 variability of marine stratocumulus clouds. *J. App. Meteor.*, **27**, 797-810.
 552 Brooks, I., 2003, Finding Boundary Layer Top: Application of a wavelet covariance
 553 transform to lidar backscatter profiles. *J. Atmos. Ocean. Tech.*, **20**, 1092-1105.
 554 Campbell, J. R., D. L. Hlavka, E. J. Welton, C. J. Flynn, D. D. Turner, J. D. Spinhirne,
 555 V. S. Scott III, and I. H. Hwang, 2002, Full-time, eye-safe cloud and aerosol lidar
 556 observation at Atmospheric Radiation Measurement program sites: Instruments and data
 557 processing. *J. Atmos. Ocean. Tech.*, **19**, 431-442.
 558 Cohn, S. A., and W. M. Angevine, 2000, Boundary layer height and entrainment zone
 559 thickness measured by lidars and wind-profiling radars. *J. App. Meteor.*, **39**, 1233-1247.
 560 Córdoba-Jabonero, C., M. Sorribas, J. L. Guerrero-Rascado, J. A. Adame, Y.
 561 Hernández, H. Lyamani, V. Cachorro, M. Gil, L. Alados-Arboledas, E. Cuevas, and B.
 562 de la Morena, 2011, Synergetic monitoring of Saharan dust plumes and potential impact
 563 on surface: a case study of dust transport from Canary Islands to Iberian Peninsula.
 564 *Atmos. Chem. Phys.*, **11**, 3067-3091, doi:10.5194/acp-11-3067-2011.
 565 Davis, K. J., N. Gamage, C. R. Hagelberg, C. Kiemle, D. H. Lenschow, and P. P.
 566 Sullivan, 2000, An objective method for deriving atmospheric structure from airborne
 567 lidar observations. *J. Atmos. Ocean. Tech.*, **17**, 1455-1468.
 568 Flamant, C., J. Pelon, P. H. Flamant, and P. Durand, 1997, Lidar determination of the
 569 entrainment zone thickness at the top of the unstable marine atmospheric boundary
 570 layer. *Bound. Layer Meteor.*, **83**, 247-284.
 571 Garratt, J. R., 1992, *The Atmospheric Boundary Layer*. Cambridge Atmospheric and
 572 Space Science Series, Cambridge Univ. Press, 335 pp.

573 Hägeli, P., D. G. Steyn, and K. B. Strawbridge, 2000, Spatial and temporal variability of
 574 mixed-layer depth and entrainment zone thickness. *Bound. Layer Meteor.*, **97**, 47-71.
 575 Hayden, K. L., K. G. Anlauf, R. M. Hoff, J. W. Strapp, J. W. Bottenheim, H. A. Wiebe,
 576 F. A. Froude, J. B. Martin, D. G. Steyn, and I. G. McKendry, 1997, The Vertical
 577 Chemical and Meteorological Structure of the Boundary Layer in the Lower Fraser
 578 Valley during Pacific '93. *J. Atmos. Environ.*, **31**, 2089-2105.
 579 Heffter, J. L., 1980, *Air Resource Laboratories atmospheric transport and dispersion*
 580 *model*. NOAA Tech. Memo. ERL ARL-81, 24 pp.
 581 Hernández-Ceballos, M. A., J. A. Adame, J. P. Bolívar, and B. de la Morena, 2013, A
 582 mesoscale simulation of coastal circulation in the Guadalquivir valley (southwestern
 583 Iberian Peninsula) using the WRF-ARW model. *Atmos. Res.*, **124**, 1-20.
 584 Hooper, W. P., and E. W. Eloranta, 1986, Lidar measurements of wind in the planetary
 585 boundary layer: The method, accuracy and results from joint measurements from
 586 radiosonde and kytoon. *J. Clim. App. Meteor.*, **25**, 990-1001.
 587 Melfi, S. H., J. D. Spinhirne, S. H. Chou, and S. P. Palm, 1985, Lidar observation of the
 588 vertically organized convection in the Planetary Boundary Layer over the ocean. *J.*
 589 *Clim. App. Meteor.*, **24**, 806-821.
 590 Menut, L., C. Flamant, J. Pelon, and P. H. Flamant, 1999, Urban boundary-layer height
 591 determination from lidar measurements over the Paris area. *App. Opt.*, **38**, 945-954.
 592 Oke, T. R., 1988, *Boundary Layer Climates*, 2nd ed., HalstedPress, New York, 435 pp.
 593 Pal S., 2014, Monitoring Depth of Shallow Atmospheric Boundary Layer to
 594 Complement LiDAR Measurements Affected by Partial Overlap. *Remote Sensing*, **6(9)**,
 595 8468-8493.
 596 Pal, S., A. Behrendt, and V. Wulfmeyer, 2010, Elastic-backscatter-lidar-based
 597 characterization of the convective boundary layer and investigation of related statistics.
 598 *Ann. Geophys.*, **28**, 825-847.

599 Piironen, A K., and E. W. Eloranta, 1995, Convective boundary layer depths and cloud
600 geometrical properties obtained from volume imaging lidar data. *J. Geophys. Res.*, **100**,
601 569-576.

602 Seibert, P., F. Beyrich, S. E. Gryning, S. Joffre, A. Rasmussen, and P. Tercier, 1998,
603 *Mixing layer depth determination for dispersion modeling*. In: COST Action 710 –
604 Final Report. Harmonization of the pre-processing of meteorological data for
605 atmospheric dispersion models, Report of Working Group 2, Office for Official
606 Publications of the European Communities, Luxembourg, 431 pp.

607 Seibert, P., F. Beyrich, S. E. Gryning, S. Joffre, A. Rasmussen, and P. Tercier, 2000,
608 Review and intercomparison of operational methods for the determination of the mixing
609 height. *Atmos. Environ.*, **37**, 1001-1027.

610 Senff, C., J. Bösenberg, G. Peters, and T. Schaberl, 1996, Remote sensing of turbulence
611 ozone fluxes and the ozone budget in the convective boundary layer with DIAL and
612 Radar-RASS: A case study. *Contributions to Atmospheric Physics*, **69**, 161-176.

613 Sicard, M., C. Pérez, F. Rocadenboch, J. M. Baldasano, and D. García-Vizcaino, 2006,
614 Mixed layer depth determination in the Barcelona costal area from regular lidar
615 measurements: Methods, results and limitation. *Bound. Layer Meteor.*, **119**, 135-157.

616 Sorbjan, Z., 1989, *Structure of the Atmospheric Boundary Layer*. Prentice Hall,
617 Englewood Cliffs, N.J., 317 pp.

618 Steyn, D. G., M. Baldi, and R. M. Hoff, 1999, The detection of mixed layer depth and
619 entrainment zone thickness from lidar backscatter profiles. *J. Atmos. Ocean. Tech.*, **16**,
620 953-959.

621 Stull, R. B., 1988, *An introduction to boundary layer Meteorology*. Kluwer Academic
622 Publishers, Dordrecht, Netherlands, 666 pp.

623 Toledo, D., C. Córdoba-Jabonero, and M. Gil-Ojeda, 2014, Cluster Analysis: A new
624 approach applied to Lidar measurements for Atmospheric Boundary Layer height
625 estimation. *J. Atmos. Ocean. Tech.*, **31** (2), 422-436.

626

627

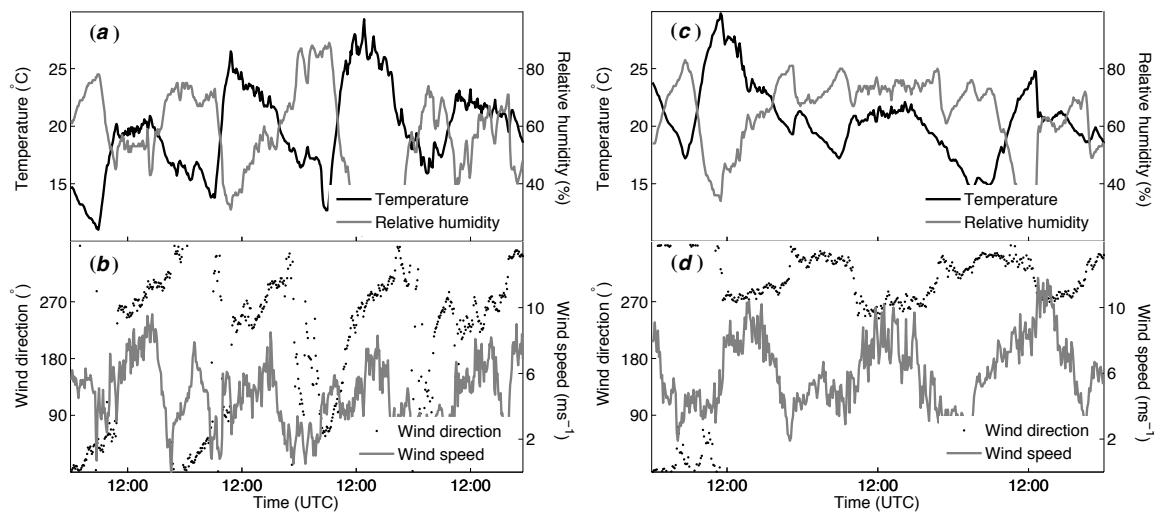


Figure 1. Surface evolution of the temperature and relative humidity and wind speed and direction (bottom) for (a-b) pure breeze conditions from 22 to 25 May 2012, and (c-d) non-pure breeze regimes from 06 to 08 June 2012.

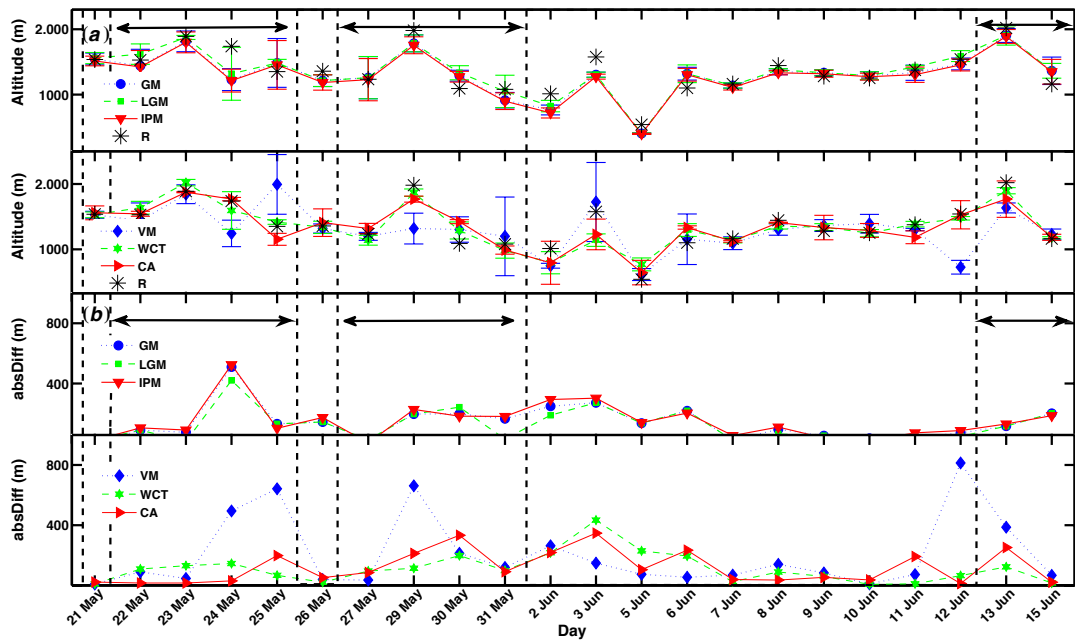


Figure 2. (a) ABL heights derived from the GM (gradient method), LGM (logarithm gradient method), IPM (inflection point method), VM (centroid/variance method), WCT (wavelet covariance transform), CA (cluster analysis) and the radiosounding retrieval (R) during the overall AMISOC-ARN campaign period. (b) Absolute differences (absDiff) between the ABL heights obtained by the radiosounding data and those calculated using the six methods. The bands delimited by the dashed lines represent the corresponding breeze regimes identified for each day to distinguish pure (indicated by double arrows) and non-pure cases.

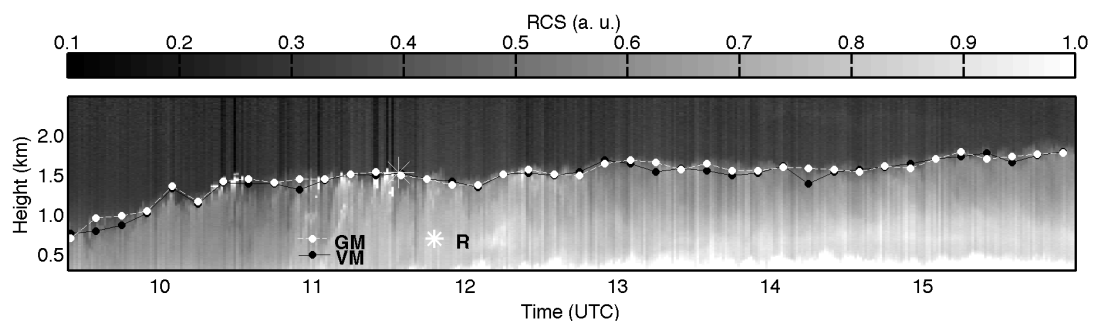


Figure 3. Temporal evolution of both the lidar RCS and the ABL top height as estimated by GM (white dots) and VM (black dots) on 21 May 2012.

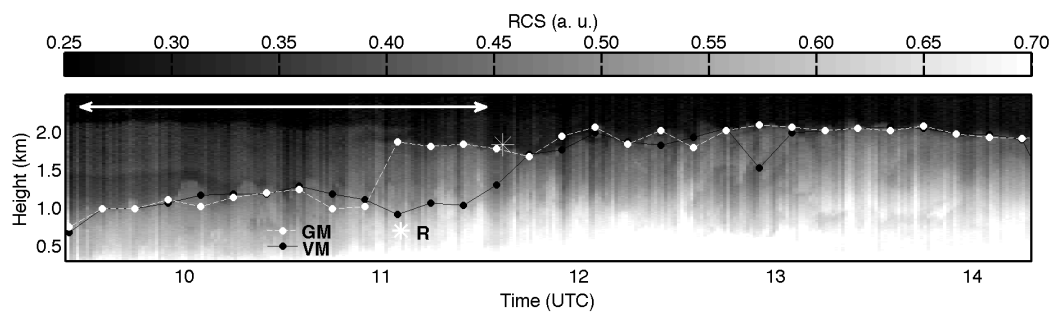


Figure 4. Same as figure Fig. 3 but on 29 May 2012. The white double arrow indicates the time interval for which a residual layer is observed.

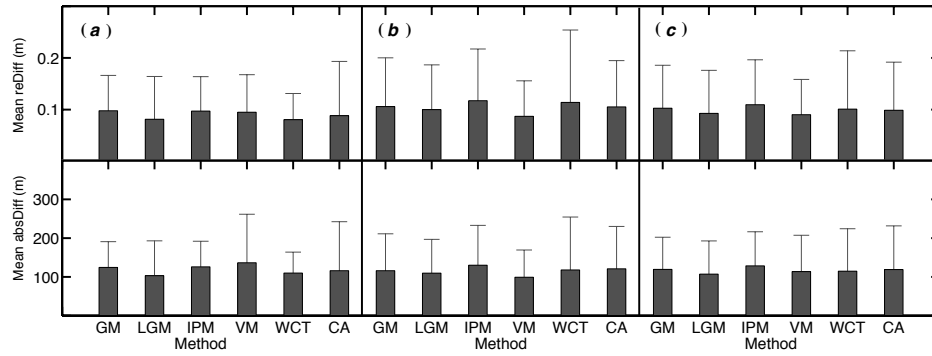


Figure 5. The mean absolute relative difference (mean reDiff) and mean absolute difference (mean absDiff) values and corresponding one standard deviation (1σ , shown by error bars) obtained by each method shown in Fig. 2 for (a) pure breeze cases, (b) non-pure breeze cases, and (c) for the overall period.

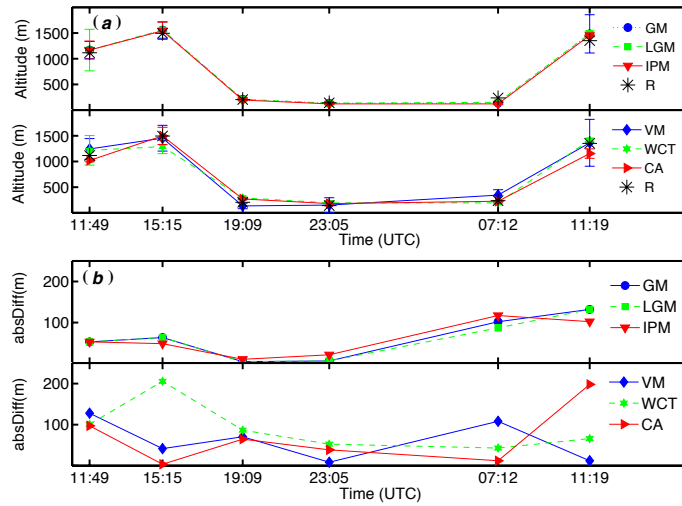


Figure 6. (a) and (b) are the same as Fig. 2a and 2b of the manuscript, respectively, but during the intensive radio soundings period corresponding to ND conditions.

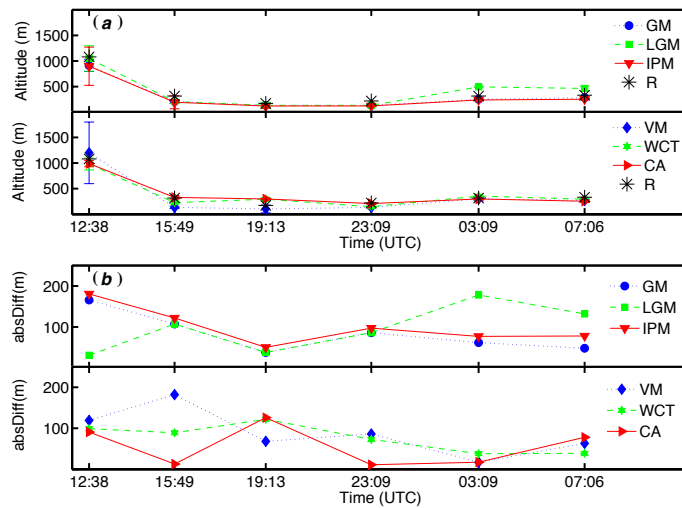


Figure 7. (a) and (b) are the same as Fig. 2a and 2b of the manuscript, respectively, but during the intensive radio soundings period corresponding to DD conditions.

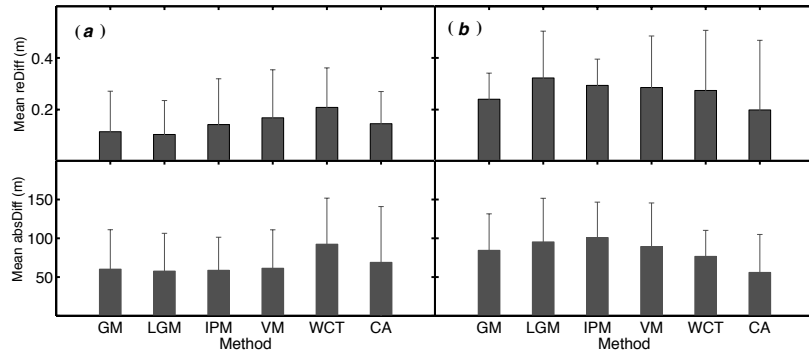
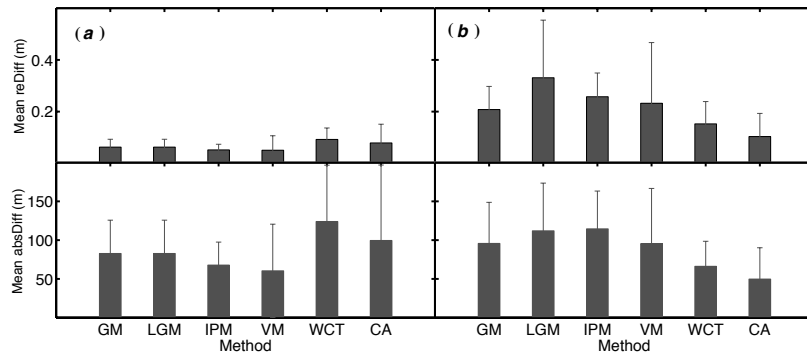


Figure 8. The same as Fig. 5, but for the aerosol conditions examined in this work: (a) ND period and (b) DD period.



748
 749 Figure 9. The same as Fig. 8 but considering in the analysis only the retrieved ABL
 750 heights greater 300 m.

751

752